

Adaptive Simmering Control for Domestic Induction Cookers

D. Paesa, C. Franco, S. Llorente, G. Lopez-Nicolas and C. Sagues

Abstract—The goal of this paper is twofold. Firstly, we aim at investigating the potentials of reset observers applied to process control. Secondly, we aim to overcome the existing performance limitations of the temperature control in domestic cookers. To this end, we present an adaptive simmering control for induction cookers, whose parameters are updated on-line depending on the estimates provided by a Multiple-Model Reset Observer (MMReO). This new observer results of extending the idea of multiple models to the state observer framework. MMReO consists of a reinitialized reset observer, and of multiple fixed identification models. The resultant control scheme satisfies the user requirements such as quick heating up, accurate temperature control, and fast disturbance rejection, outperforming previous results. Moreover, the proposed control scheme reduces energy consumption and, consequently, it can increase the efficiency of the whole cooking process. Additionally, a fixed robust QFT-based controller is designed, and it is also used for comparison purposes. Several verification tests are carried out in real induction hobs, to underline the effectiveness of our proposal compared with the QFT-based controller.

Index Terms—Adaptive Control, Robustness, Induction Heating, Observers, Temperature Control, Home Appliances.

I. INTRODUCTION

In domestic induction cookers, an inverter topology supplies a high-frequency current to an induction coil, producing an alternating magnetic field. If this field is applied to a ferromagnetic pan, it produces eddy currents, and magnetic hysteresis, which heat up the pan. Recently, domestic induction hobs have become increasingly popular thanks to their specific features such as quick warming, energy saving, and high efficiency. Consequently, the research on induction cookers has attracted the attention of theory specialists, and practical engineers [1].

The effort to increase the efficiency, and the energy saving during a cooking process using an induction hob has been mainly focused on providing to the pot the maximum power in the more efficient way. For instance, designing highly efficient resonant inverter topologies [2], modulation strategies [3], and inductors [4].

However, since user has no any feedback about how high the temperature is, user tends to use more power than the cooking process actually needs. This waste of energy

This work was supported in part by DGA project PI065/09 and BSH Home Appliances Group.

D. Paesa, C. Franco, G. Lopez-Nicolas and C. Sagues are with Departamento de Informatica e Ingenieria de Sistemas / Instituto de Investigacion en Ingenieria de Aragon, Universidad de Zaragoza, Spain. e-mail: dpaesa@unizar.es, cfranco@unizar.es, gonlopez@unizar.es, csagues@unizar.es

S. Llorente is with the Research and Development Department, Induction Technology, Product Division Cookers, BSH Home Appliances Group, 50016, Zaragoza, Spain. e-mail: sergio.llorente@bshg.com

highly decreases the efficiency of the whole cooking process, although the efficiency of the power electronics is very high. Therefore, an improvement in the efficiency during the whole cooking process could be achieved by means of pot temperature control. Besides, it has more advantages. For instance, pot temperature control ensures a correct food cooking minimizing the cooking time, and avoiding to reach too high temperatures, which burn the food, or too low temperatures, which cause underdone food. Additionally, it can be used to perform more complicated cooking process such as simmering. During simmering, the food is submerged in water at a temperature from 88°C to 94°C which causes a great effect on the flavour of food. However, it is almost impossible to carry out in conventional cookers where user does not control the temperature of the cooking pot.

The first work related to pot temperature control for induction hobs is [5]. There the authors developed a temperature control for frying pans. Since the pan temperature was not directly measured, it had to be estimated from the measurements of a NTC sensor situated below the ceramic glass. However, that measurement was highly dependent on the cooking load. Therefore, it did not work properly with high-load cooking process such as boiling and deep frying. This problem does not appear when using the external infrared sensor proposed in [6], rather than a NTC sensor. This approach guarantees an accurate measurement of the pot wall temperature, and it was successfully applied to radiant hobs in [7]. Fig. 1 shows the lay-out of both sort of sensors used in domestic induction hobs. It is worth mentioning that in this work, the measurements of the NTC sensor are not used, and the proposed control strategies only relay on the external infrared sensor.

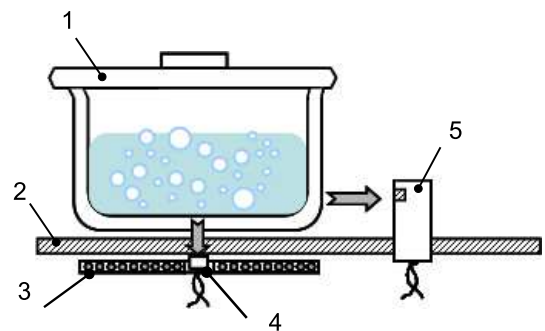


Fig. 1. Main elements of a domestic induction hob. 1: pot. 2: ceramic glass. 3: induction coil. 4: internal NTC sensor. 5: external infrared sensor

In this paper, we present an adaptive simmering control for domestic induction cookers. It is based on an infrared

sensor rather than on a NTC sensor, and consequently, it can be applied to high-load cooking process unlike other previous works [5]. Our proposal exploits the potential benefits of using an accurate model of the system [8]. One of the contributions of this work compared with [7], is that our control strategy is based on an analytical model of the system rather than on multiple experimental tests, and consequently, the controller tuning process is highly simplified. Specifically, we propose an adaptive controller whose parameters are updated on-line depending on the estimates provided by a Multiple-Model Reset Observer (MMReO). It consists of a reinitialized reset observer, which is a novel sort of observer recently proposed by the authors, and of multiple fixed identification models, which estimate the best initial parameters of the reset observer. For this reason, this paper also contributes at analyzing the potentials of reset observers applied to process control. Furthermore, for comparison purposes, we have designed a fixed robust QFT-based controller, which is a control technique widely applied to industrial applications. To highlight the performance of our proposal, both control schemes have been implemented in a real induction hob, and several verification tests have been carried out.

This paper is organized as follows. In Section II, the state space model of the system is presented. In Section III, the adaptive MMReO-based controller design is given. After that, the tuning process of the fixed QFT robust controller is outlined in Section IV. Experimental results are shown in Section V in order to test the robustness and performance of both control schemes. Finally, concluding remarks are outlined in Section VI.

II. SYSTEM MODEL

State space model can be used to represent the relation between the power supplied by the induction coil, and the temperatures of the system. Generally, linear time invariant systems are described as follows

$$\begin{aligned} \dot{x}(t) &= A \cdot x(t) + B \cdot u(t) \\ y(t) &= C \cdot x(t) \end{aligned} \quad (1)$$

where $x(t) \in \mathbb{R}^n$ is the state vector, $u(t) \in \mathbb{R}^l$ is the input vector, $y(t) \in \mathbb{R}^m$ is the system output vector, and A, B, C are constant $(n \times n), (n \times l), (m \times n)$ matrices.

In this paper, we use the analytical pot model presented in [8]. Thus, readers interested in how that system is obtained are referred there. The main idea is that, by using an electrical equivalent model that represents the different heat transmissions which appear in our system, it is possible to obtain the following state space model:

$$\begin{aligned} \begin{bmatrix} \dot{\theta}_B \\ \dot{\theta}_W \end{bmatrix} &= \begin{bmatrix} a_{11} & a_{12} \\ a_{21} & a_{22} \end{bmatrix} \begin{bmatrix} \theta_B \\ \theta_W \end{bmatrix} \\ &+ \begin{bmatrix} b_{11} & 0 \\ 0 & b_{22} \end{bmatrix} \begin{bmatrix} P \\ Q_E \end{bmatrix} \\ \theta_W &= \begin{bmatrix} 0 & 1 \end{bmatrix} \begin{bmatrix} \theta_B \\ \theta_W \end{bmatrix} \end{aligned} \quad (2)$$

TABLE I
NOMINAL MODEL PARAMETERS AND THEIR RANGES

Parameter	Nominal Value	Variations
a_{11}	-0.0197	[-0.0461 -0.0048]
a_{12}	0.0097	[0.00230 0.02291]
a_{21}	0.0018	[0.00030 0.00540]
a_{22}	-0.0010	[-0.0029 -0.0002]
b_{11}	0.0018	[0.00120 0.00290]
b_{22}	0.0001	[0.00010 0.00040]

where $\theta_B = T_B - T_0$ is the difference between the pot bottom temperature T_B and the ambient temperature, $\theta_W = T_W - T_0$ is the difference between the pot wall temperature T_W and the ambient temperature, P is the power supplied by the inductor coil which takes into account the efficiency of the electronics and of the inductor, and Q_E is the energy loss because of evaporation. Additionally, $a_{11}, a_{12}, a_{21}, a_{22}, b_{11}$, and b_{22} are uncertain parameters that depend on the pot and glass thermal properties, as well as on the different thermal losses of the system. Namely, convection, radiant, and conduction losses.

Since the pot which is being used during the simmering process is unknown, these uncertain parameters are initially unknown. However, according to our results obtained from simulations, the value of each uncertain parameter is within a known variation range. Table I summarizes the nominal values of all model parameters and their variations obtained from a study of 150 different pots.

Notice that most of cooking processes are carried out using a lid, because it highly decreases the thermal losses of the system, and consequently, improves efficiency. Therefore, we consider that the simmering cooking process is done in a pot covered with a lid which implies that $Q_E = 0$. It is also worth mentioning that the pot bottom temperature T_B cannot be directly measured, therefore an observer scheme is needed in order to estimate \hat{T}_B . Since the output of the system (i.e. T_W) is the variable to control, T_B is not strictly needed for control purposes. That is the way in which the QFT-based controller is designed. However, better performance would be obtained, if all the state variables were known or estimated. Thus, the MMReO-based controller relies on the state space model (2), considering all the state variables.

III. ADAPTIVE MMREO-BASED CONTROLLER

Robust control techniques such as QFT or H_∞ can be regarded as conservative, due to the fact that the resultant controller has to be designed to meet control requirements, for the worst-case behavior between all the considered operation points (i.e. for all the uncertainty of the system). Therefore we could obtain a better performance, if we were able to reduce the uncertainty of the cooking process somehow.

Adaptive observers can play a key role in this approach, since they have been widely used to estimate the unknown parameters of a system from the information available (e.g. system input and output measurements) [9]. Therefore, this sort of algorithms represents a useful tool in order to cope

with problems that may appear in any industrial application. For instance, they can be used to deal with systems whose parameters are initially unknown due to modeling uncertainties, and also to handle systems whose parameters are time variant. Additionally, they have important applications not only in adaptive control but also in fault detection and isolation [10].

Among the different sort of adaptive observers, we present an estimation strategy that relays on multiple models of the system, in order to increase the robustness of the estimation process. The idea of multiple models was firstly introduced for control purposes [11]. It is commonly accepted that the convergence time of an adaptive control scheme will be large if the initial parameter of the controller are not close enough to the plant parameters. This transient behavior can be improved using multiple models [12], [13]. Assuming that the plant parameters belong to a compact set S , this approach relays on using N identification models with different parameters but uniformly distributed in S . A controller for each model is also calculated and tuned. Therefore, the proposed strategy is to determine the best model for the real system at every instant, and using the corresponding controller to control the plant.

Build on [12], we extended the idea of multiple models to the state observer framework. The resultant observer scheme is denoted as Multiple Model Observer (MMO). In a similar way, N identification models with different parameters but uniformly distributed in S are used to estimate the best model for the real system. At every instant, the parameters of the best identified model are used as the starting parameters of an additional state observer. This process is known as the reinitialization of the state observer. Since the reinitialized parameters of the state observer are closer to the real ones, the convergence time of the estimation process is decreased. Afterwards, the state estimated by the reinitialized observer can be used in the control law. Furthermore, the parameters corresponding to the best identified model can also be used to adapt the control law, to improve even more the closed-loop response of the system.

Based on this approach, we present in this paper an adaptive controller whose parameters are updated on-line depending on the estimates provided by a Multiple-Model Reset Observer (MMReO). MMReO scheme is depicted in Fig. 2. It consists of a reinitialized reset observer, and of multiple fixed identification models. Each fixed identification model has the structure shown in (2) with different parameters a_{11} , a_{12} , a_{21} , a_{22} , b_{11} , and b_{22} defined according to Table I, which actually define the convex set S for our system. The behavior of the MMReO scheme is as follows. It selects the identification model that best represents the cooking process depending on the output of the system y (i.e. the temperature measured with the infrared sensor), and the input of the system u (i.e. the power supplied with the induction coil). Specifically, the algorithm uses the following

cost function J_i to find out the best model $i \in [1, N]$

$$J_i = \epsilon_i^2(t) + \int_{t=0}^{t=\infty} \epsilon_i^2(t) dt \quad (3)$$

where $\epsilon_i(t) = y(t) - \bar{y}_i(t)$ is the identification error of the model i defined as the difference between the output of the system $y(t)$ and the output of the identification model $\bar{y}_i(t)$. The algorithm also generates a switching signal σ that is used to update the parameters of the reinitialized reset observer. Since the observer parameters are closer to the real system parameters, it is expected to decrease the transient behavior of the observer and, as a consequence, to improve the control performance which relays on the estimated state.

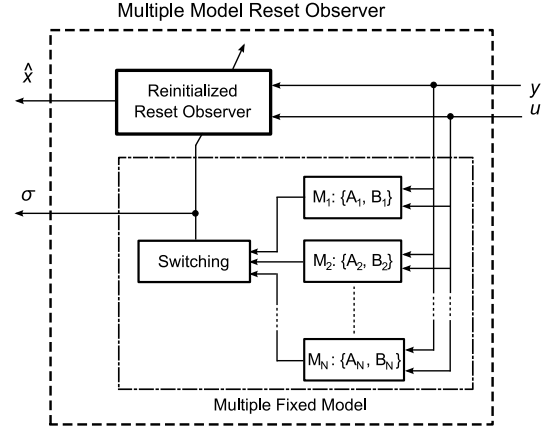


Fig. 2. Multiple Model Reset Observer Scheme.

As it is shown in Fig. 2, we use a reset observer (ReO) whose matrices \bar{A} , \bar{B} are reinitialized according to the matrices of the best model chosen. The aim of the ReO is to estimate the system state variables (i.e. $\hat{x} = [\hat{\theta}_B, \hat{\theta}_W]$), which will be used afterwards in the control law. The ReO dynamics are described as follows [14]

$$\begin{aligned} \dot{\hat{x}} &= \bar{A}\hat{x} + \bar{B}u + K_I\zeta + K_P\tilde{y} \\ \hat{y} &= C\hat{x} \end{aligned} \quad (4)$$

where \hat{x} is the state estimated by the ReO, K_I and K_P represent the integral and proportional gain of the ReO respectively, and $\tilde{y} = y - \hat{y}$ is the output estimation error of the ReO, \bar{A} and \bar{B} are the system matrices associated with the best model previously identified. In addition, ζ is the reset integral term which is computed as

$$\begin{aligned} \dot{\zeta} &= A_\zeta\zeta + B_\zeta\tilde{y} & \tilde{y} \cdot \zeta \geq 0 \\ \zeta^+ &= A_r\zeta & \tilde{y} \cdot \zeta \leq 0 \end{aligned} \quad (5)$$

where $A_\zeta \in \mathbb{R}$ and $B_\zeta \in \mathbb{R}$ are two tuning scalars which regulate the transient response of ζ , and A_r is the reset matrix.

Regarding (5), ReO can be seen as an hybrid observer with a *flow* and a *reset* state, and the two conditions at the right side are the *flow* and the *reset* condition respectively. On one hand, as long as $\tilde{y} \cdot \zeta \geq 0$ the observer behaves as a proportional integral observer. On the other hand, if $\tilde{y} \cdot \zeta \leq 0$, the integral term is reset according to the reset map A_r .

Recent results have highlighted the potential benefit of including a reset element in the estimation laws. Since the ReO is mainly nonlinear, it can meet requirements that cannot be satisfied by pure linear observers. Namely, reset elements can decrease the overshoot, and settling time of the estimation process without sacrificing the rise time. Readers interested in the stability, and convergence analysis of the ReO as well as in how to select the tuning parameters of the ReO are referred to [14].

Once the estimation process is done (i.e. when \hat{x} has been computed), the parameters of the adaptive controller are updated depending on the identified model. An adaptive PI controller is selected because of its simplicity and easy auto-tuning. Fig. 3 shows the proposed adaptive control scheme, whereas the designed control law is

$$\begin{aligned} u &= L_I x_I - L_S \hat{x} \\ \dot{x}_I &= r - y \end{aligned} \quad (6)$$

where r is the target temperature, x_I is the integral error, L_I and L_S are the integral gain of the controller and the state gain of the controller respectively, which are off-line computed with pole placement method, and afterwards, are updated on-line through a look-up table depending on the best model identified with the MMReO scheme.

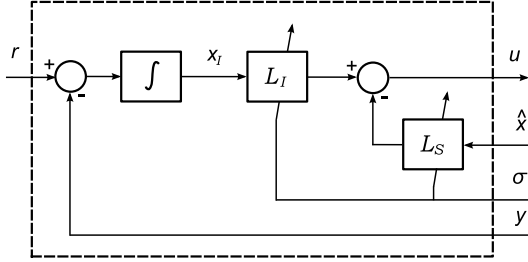


Fig. 3. Adaptive Control Scheme.

It is worth mentioning that since we have implemented $N = 60$ fixed identification models, we do not include here for brevity all the values of the parameters involved in this control scheme that depend on the identified model (e.g. A_i , and B_i in the MMReO scheme; L_I , and L_S in the adaptive control scheme).

To give insights into the behavior of the proposed adaptive control based on MMReO, we show some simulation results obtained with the simulator developed from [8]. We aim at heating up a cooking pot filled with 1 liter of water from ambient temperature (i.e. 25°C) to the target temperature (i.e. 91°C).

Fig. 4 shows the parameters of the best model identified minimizing the cost function (3) at every instant. Since the number of fixed identification models is finite there still exists a small difference between the best model and the real system. Nonetheless, identified parameters are close enough to real ones in such a manner that the convergence speed of the reinitialized reset observer is highly decreased. Fig. 5 shows the temperatures of the cooking process as well as the temperatures estimated by the ReO. It underlines the good

performance of the MMReO, since both temperatures are properly estimated.

Additionally, Fig. 6 shows the action computed by using the control law (6), which relays on the temperatures estimated by the ReO. It is evident the good performance of the whole control scheme, since T_W reaches the target temperature without overshooting as it is shown in Fig. 5. Finally, Fig. 7 shows the reset integral term ζ , and how it is reset at $t = [200, 310, 550]$. These resets as well as the reinitializations of the state observer, cause small discontinuities in the temperature of the bottom of the pot estimated by the ReO, and thus, in the action computed by the adaptive controller, as it is shown in Fig. 6. However, these discontinuities allow the water temperature to reach the desired reference, minimizing rise time and overshoot.

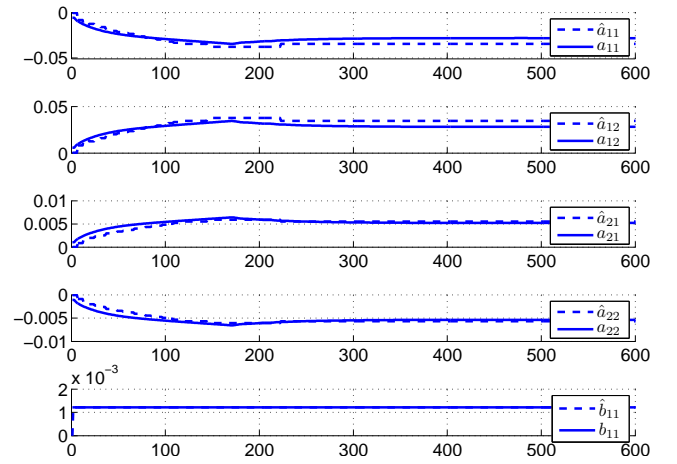


Fig. 4. Simulation Results with the adaptive controller based on MMReO. Solid lines are the parameters a_{11} , a_{12} , a_{21} , a_{22} , b_{11} . Dashed lines are the estimated parameters \hat{a}_{11} , \hat{a}_{12} , \hat{a}_{21} , \hat{a}_{22} , \hat{b}_{11} . Notice that, since it is assumed $Q_E = 0$, the effect of $Q_E \cdot b_{22}$ is negligible for all b_{22} . Therefore, b_{22} is not estimated on-line but set to the nominal value during all the tests.

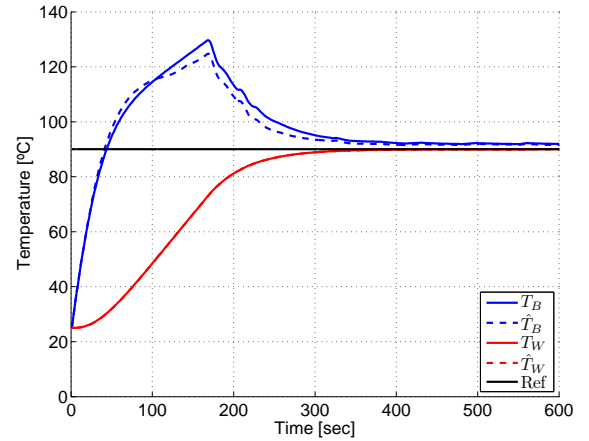


Fig. 5. Simulation Results with the adaptive controller based on MMReO. T_B is the temperature of the bottom of the pot, \hat{T}_B is the estimated temperature of the bottom of the pot, T_W is the temperature measured with the infrared sensor, \hat{T}_W is the estimated temperature of the wall of the pot which is almost equal to T_W , Ref is the target temperature.

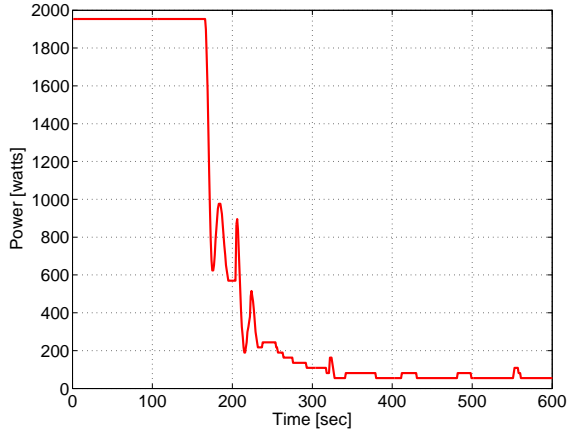


Fig. 6. Simulation Results with the adaptive controller based on MMReO. Power computed with the control law (6) which depends on the state estimated with the ReO.

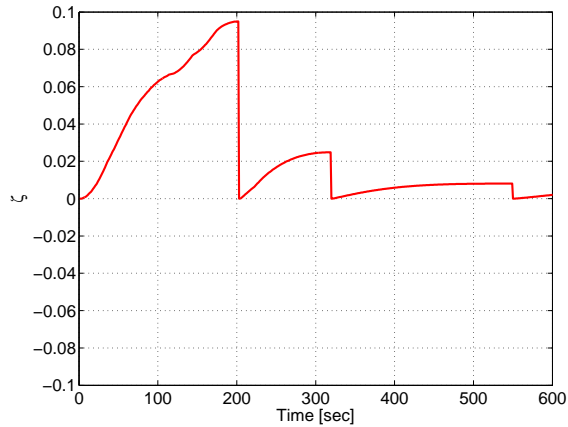


Fig. 7. Simulation Results with the adaptive controller based on MMReO. Reset integral term ζ computed with the ReO. When ζ is reset to zero, it means that the reset condition holds.

IV. FIXED QFT-BASED CONTROLLER

We also present here a fixed QFT-based controller, which does not need estimation of variable T_B , and it is used for comparison with the adaptive MMReO-based controller.

Quantitative Feedback Theory (QFT) is a robust control technique developed by Isaac Horowitz [15]. It has been widely used in industrial applications for the last three decades [16], [17], because it takes into account system parameter uncertainty in the design of the controller. It has been recently applied to simmering control for induction cookers in [18], and here we summarize how that controller was designed, for the paper to be self-contained.

The first step in QFT design is to translate the system uncertainty to frequency domain. For this purpose, the frequency responses of all possible combinations of system parameters are represented in a Nichols chart. Each point plotted represents a possible plant or sensor for a given frequency. Therefore all these points define a region of the uncertainty of the system at the different working frequencies. These regions are known as templates. In particular, the templates obtained for the uncertain system described in Table I

for the working frequencies $w = [0.002, 0.005, 0.02, 0.1, 1]$ rad/s are shown in Fig. 8.

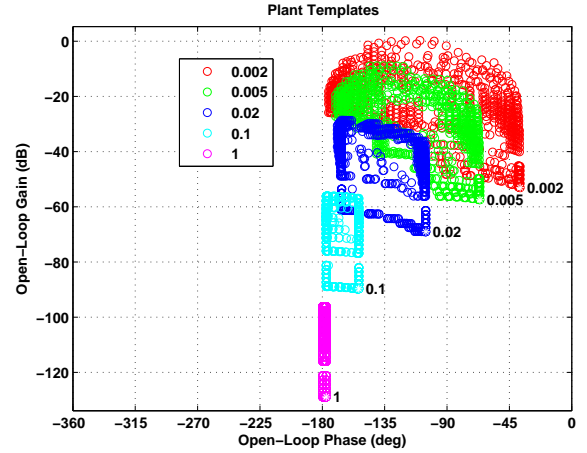


Fig. 8. Plant templates at the working frequencies $w = [0.002, 0.005, 0.02, 0.1, 1]$ rad/s.

In the next step, control requirements have to be translated into boundaries in a Nichols chart. In QFT, each closed-loop specification, such as robust stability, tracking ability, and disturbance rejection, generates a boundary. If the nominal open loop avoids the boundaries, it is guaranteed that the closed loop specifications are satisfied for all the plants considered in the template.

For our system, we have selected the following closed-loop performance specifications:

- 1) *Robust Stability*: To ensure robust stability of the closed-loop system, the following constraint on the peak magnitude of the closed loop frequency response is set:

$$\left| \frac{P(s)G(s)}{1 + P(s)G(s)} \right| \leq \gamma \quad (7)$$

where $P(s)$ is the plant, and $G(s)$ is the controller. Moreover, γ is the maximum peak magnitude which corresponds to a minimum gain margin (GM), and phase margin (PM), [19] as follows:

$$GM = 20 \log \left(\frac{\gamma + 1}{\gamma} \right) [dB] \quad (8)$$

$$PM = 2 \sin^{-1} \left(\frac{1}{2\gamma} \right) [deg] \quad (9)$$

in particular, we have chosen $\gamma = 1.5$ which gives $GM = 4.43$ and $PM = 39^\circ$.

- 2) *Reference Tracking*: Due to system uncertainty, we define an acceptable range of variations in the closed loop tracking responses. According to [20], [21], we define an upper $T_{UP}(s)$, and lower $T_{DW}(s)$ bounds for the closed-loop response of our system as follows:

$$|T_{DW}(s)| \leq \left| \frac{P(s)G(s)}{1 + P(s)G(s)} \right| \leq |T_{UP}(s)| \quad (10)$$

Specifically, we have selected the following tracking bounds

$$T_{UP}(s) = \frac{1.02}{(20s + 1)(5s + 1)} \quad (11)$$

$$T_{DW}(s) = \frac{0.98}{(80s + 1)(70s + 1)(1s + 1)(0.1s + 1)} \quad (12)$$

3) *Plant input noise rejection:* According to (2), the power supplied by the inductor is the input of our system which is measured with a Sigma-Delta analog-to-digital converter implemented in the ASIC of the induction hob [22]. Since this converter has a measurement error about a 5%, we have designed a controller able to reject this kind of disturbances. In particular, we have chosen the following input noise rejection specification:

$$\left| \frac{P(s)}{1 + P(s)G(s)} \right| \leq 0.01 \quad (13)$$

Fig. 9 shows the intersection of these three performance specifications at the design frequencies used during the template generation. To satisfy performance specifications, the open-loop response has to be above the corresponding boundary as long as it is drawn in solid line, whereas if the boundary is drawn in dashed line the open-loop response has to be below the boundary.

It is easy to see that the system does not meet the performance specifications since the open-loop frequency response is below the performance specification bounds at each frequency. Therefore, we have to modify the system response adding poles and zeros, until the nominal loop lies near its bounds and results in nominal closed-loop stability. This process is known as loop-shaping, and generates directly the robust feedback compensator.

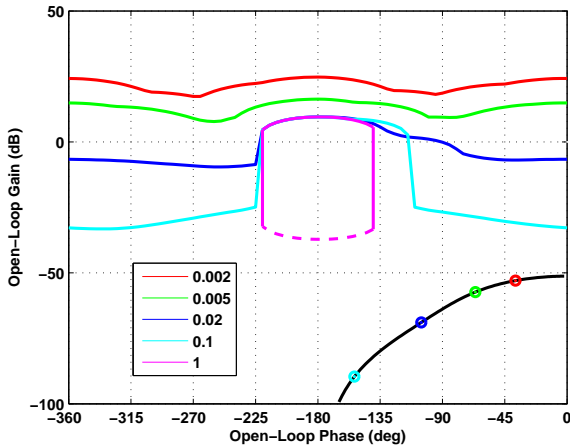


Fig. 9. Open-loop frequency response and performance specification bounds. To meet the control requirements, the nominal open loop has to avoid the boundaries.

Fig. 9 also points out that an appropriate control gain should be introduced to push the open-loop frequency response upwards. Additionally, a dynamic compensator is

required in order to change the shape of the open-loop frequency response too. Following this approach, the resulting controller is:

$$G(s) = 9 \frac{\left(\frac{1}{0.0028}s + 1\right) \left(\frac{1}{0.035}s + 1\right)}{s \left(\frac{1}{0.9}s + 1\right)} \quad (14)$$

whose frequency response with the plant is illustrated in Fig. 10. It is clearly seen that the open-loop frequency response meets now all performance requirements, since it is above all bounds at the corresponding frequency. Therefore, we can state that the designed controller ensures robust stability, and an appropriate noise rejection for all of the family of plants defined under the uncertainty shown in Table I.

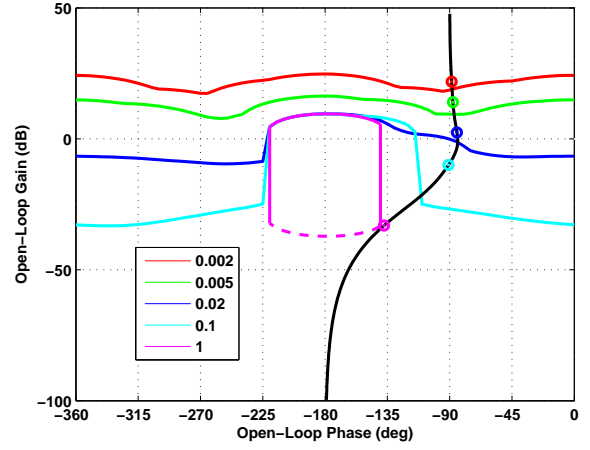


Fig. 10. Open-loop frequency response with the controller. To meet the control requirements, the nominal open loop has to avoid the boundaries.

Nevertheless, the controller is not able to satisfy the tracking specification as it is shown in Fig. 11. Therefore, a dynamic pre-filter is required to shape the frequency response to be within the required envelope, and attenuate high frequency peaking. Specifically, we have designed the following pre-filter:

$$F(s) = 1 \frac{\left(\frac{1}{0.3}s + 1\right)}{\left(\frac{1}{0.017}s + 1\right) \left(\frac{1}{0.1}s + 1\right)} \quad (15)$$

which allows to meet now the tracking specification as it is shown in Fig. 12.

So far, we have only ensured that the proposed controller meets the performance requirements at some discrete frequencies. Consequently, an additional checking step at all frequencies inside the working range is needed. For this reason, we show in Figs. 13, 14 and 15 the closed-loop response of the system with the designed controller and pre-filter for the robust stability, reference tracking, and noise rejection specifications respectively.

Concluding, the proposed fixed QFT-based controller meets the robust stability, and noise rejection specifications at all frequencies, since the closed-loop response is below the corresponding boundary in both cases (see Fig. 13 and Fig. 15). Additionally, it satisfies also the reference tracking

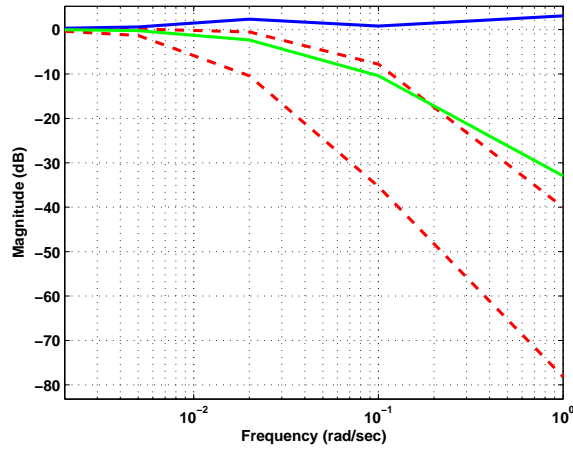


Fig. 11. Closed-loop frequency response with the controller. Red dashed lines are the reference tracking boundaries. Blue solid line is the *upper* closed-loop response. Green solid line is the *lower* closed-loop response. To meet the tracking requirement, both closed-loop responses must be within the reference tracking boundaries.

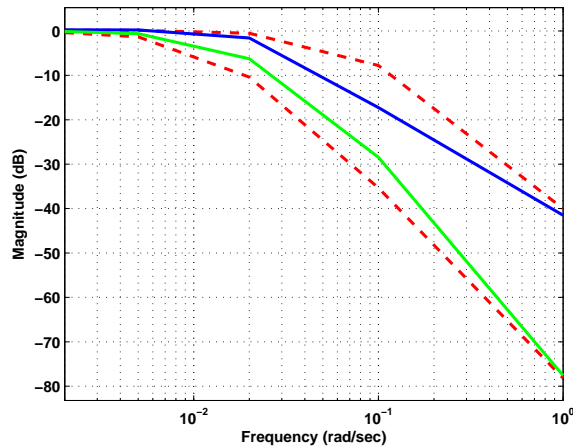


Fig. 12. Closed-loop frequency response with the controller and the pre-filter. Red dashed lines are the reference tracking boundaries. Blue solid line is the *upper* closed-loop response. Green solid line is the *lower* closed-loop response. To meet the tracking requirement, both closed-loop responses must be within the reference tracking boundaries.

specification, since the maximum and minimum closed-loop response are inside the tracking range defined in (12).

V. EXPERIMENTAL RESULTS

Both proposed controllers have been implemented in the microcontroller of a real induction hob. Specifically, these algorithms have been programmed in C language. In order to verify that the designed control schemes work properly, several verification tests on real induction hob were done. Main elements of the induction hob used are shown in Fig. 16 while the real hob used during the verification tests is shown in Fig. 17.

The induction heating process in a domestic hob comes up as follows. Hob takes the energy from the mains voltage; after that, an electromagnetic compatibility filter removes the

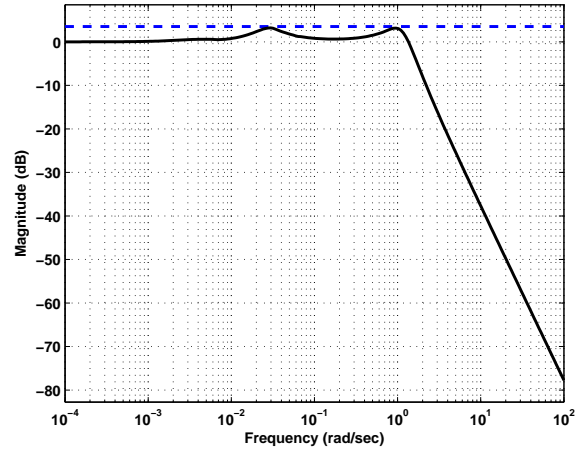


Fig. 13. Closed-loop stability margins. Blue dashed line is the closed-loop stability boundary. Black solid line is the closed-loop stability response.

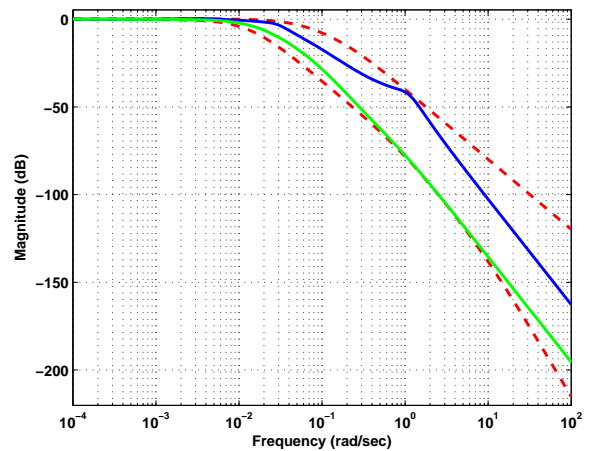


Fig. 14. Closed-loop reference tracking margins. Red dashed lines are the reference tracking boundaries. Blue solid line is the *upper* closed-loop response. Green solid line is the *lower* closed-loop response.

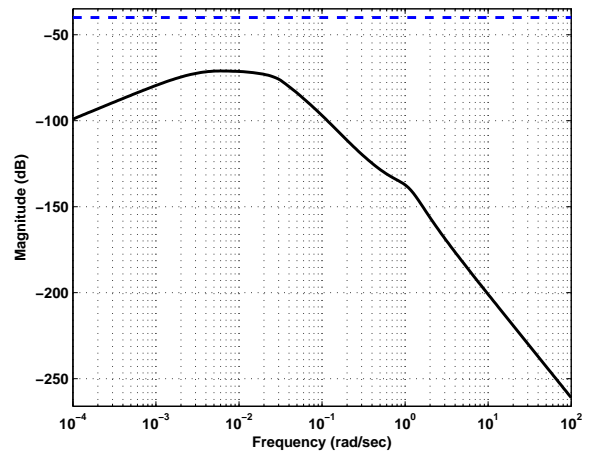


Fig. 15. Closed-loop noise rejection margins. Blue dashed line is the closed-loop noise-rejection boundary. Black solid line is the closed-loop noise-rejection response.

voltage disturbances, which is subsequently rectified by a full bridge of diodes. Finally, the inverter topology provides to the induction coil the high-frequency current needed to heat up the vessel. Since power supplied depends on it (the lesser the frequency, the higher the power), the microcontroller modifies the working frequency of the inverter to provide the desired power. The frequency control algorithm used is described in [23]. The changes of the working frequency are taken in fixed and small steps, which ensures stability and convergence of the frequency control algorithm but which causes a transient behavior before the algorithm determines the proper working frequency. Nevertheless, it has no effect in the temperature control, due to the fact that the thermal dynamics are much slower than the inverter topology dynamics (less than one second).

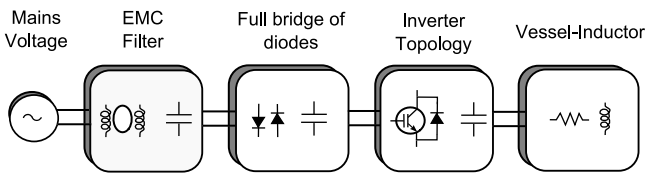


Fig. 16. Arrangement of the induction hob.



Fig. 17. Domestic induction hob used during verification test.

During verification tests, the temperature evolution of the water during a simmering process is measured. It has to reach a settling temperature between 88°C and 94°C . The software of the microcontroller automatically calculates how much power is needed in order to reach the set point with the minimum rise time but without overshoots. To check the system behavior, we measure the water temperature with an additional thermocouple situated inside the water during all the test. Notice that the software does not use the temperature measured by the thermocouple. Therefore, this thermocouple is not used in household conditions.

Figs. 18-23 show some of the results obtained with both control schemes during the verification tests. We have used a 180mm-diameter induction coil whose maximum power is 1800 watts. The objective is to heat up a predefined amount

of water until the simmering temperature as fast as possible. After that, each controller has to keep the water temperature inside the simmering range.

Fig. 18 and Fig. 19 show the results obtained with the QFT-based controller when the initial amount of water is 1.5 liters and 2.5 liters respectively. On the other hand, Fig. 21 and Fig. 22 show the results obtained with the adaptive controller based on MMReO when the initial amount of water is 1.5 liters and 2.5 liters respectively. It is worth mentioning that in all these tests the pot was covered with a lid, so that $Q_E = 0$.

Analyzing those figures, it is easy to see that both proposed controllers meet control requirements because the water reaches the simmering temperature without overshooting independently of the initial amount of water. However, the adaptive controller based on MMReO has a better performance as long as we compare the rising time. Depending on the initial amount of water, up to a 30% time saving is achieved by using the adaptive scheme presented in Section III.

Additionally, we have tested the robustness of each controller dealing with disturbances. Two different sort of disturbances have been considered. Firstly, we have performed these tests without a lid, and thus Q_E is not longer negligible (i.e. $Q_E \neq 0$), which as a matter of fact was an assumption for the tuning of both controllers. Secondly, we have also considered typical disturbances that take place during any cooking process because of the addition of food. Specifically, they have been simulated adding 0.5 liters of water to the pot after the water temperature has reached the simmering temperature. Fig. 20 shows the results obtained with the QFT-based controller whereas Fig. 23 shows the results obtained with the adaptive controller based on MMReO. Both controllers show a good behavior since both are able to keep the water temperature within the simmering range even after more water is added to the pot. Nevertheless, the adaptive controller based on MMReO outperforms again the fixed QFT-based controller, since the disturbance rejection time is significantly decreased. Specifically, it is up to 50 seconds shorter which represents about a 33% time reduction.

Regarding energy consumption, since both control schemes avoid overshooting, no energy is wasted to evaporate water. For comparison purposes, let us analyze energy consumption of induction cookers without temperature control, and with temperature control. Let assume that the user selects the maximum power level during all the test (i.e. 1800 watts), in order to heat up 2.5 liters of water for 20 minutes, in the induction cooker without temperature control. In this case, the energy consumption would be $600\text{ W} \cdot \text{h}$. On the other hand, the induction cooker with the QFT-based controller would consume $265.55\text{ W} \cdot \text{h}$ to perform the same process, whereas the induction cooker with the adaptive MMReO control would only need $260.33\text{ W} \cdot \text{h}$. This result underlines the fact that temperature control can play a key role reducing energy consumption and, as a consequence, it can increase the efficiency of the whole cooking process.

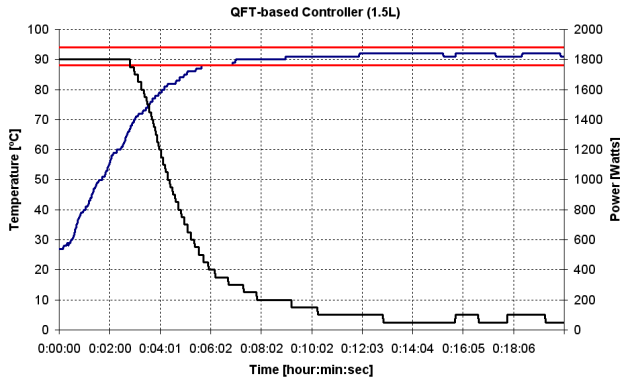


Fig. 18. Experimental results obtained with the fixed QFT-based controller. It has to heat up 1.5 liters of water to the simmering range. The pot is covered with a lid. Black line represents the supplied power. Blue line represents the water temperature measured with a thermocouple. Area between red lines represents the simmering range.

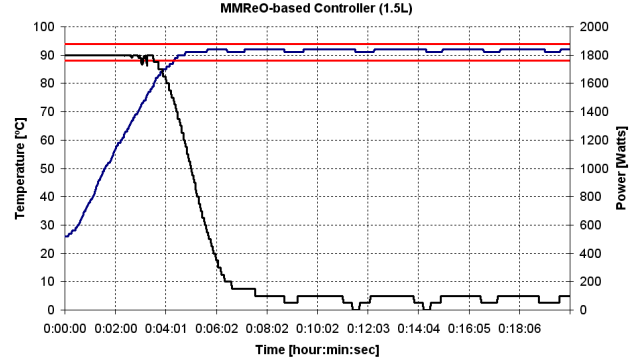


Fig. 21. Experimental results obtained with the adaptive MMReO-based controller. It has to heat up 1.5 liters of water to the simmering range. The pot is covered with a lid. Black line represents the supplied power. Blue line represents the water temperature measured with a thermocouple. Area between red lines represents the simmering range.

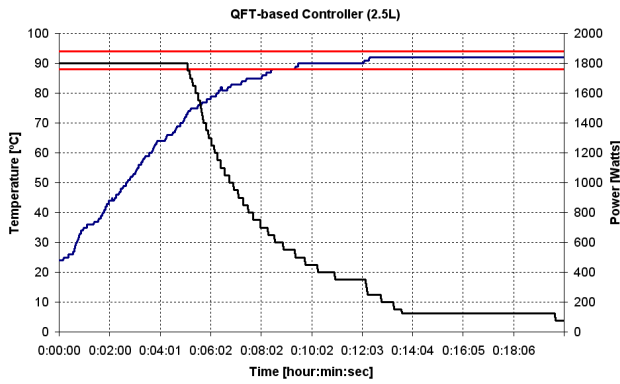


Fig. 19. Experimental results obtained with the fixed QFT-based controller. It has to heat up 2.5 liters of water to the simmering range. The pot is covered with a lid. Blue line represents the water temperature measured with a thermocouple. Area between red lines represents the simmering range.

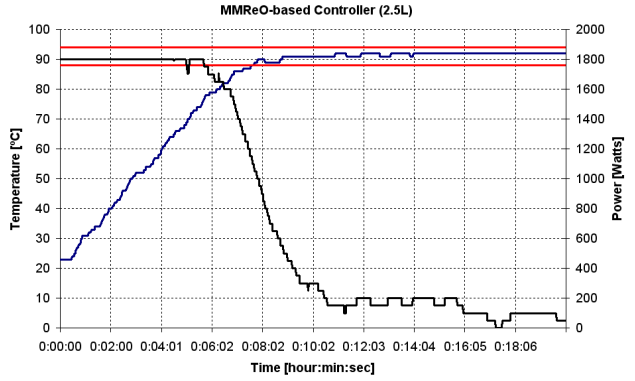


Fig. 22. Experimental results obtained with the adaptive MMReO-based controller. It has to heat up 2.5 liters of water to the simmering range. The pot is covered with a lid. Blue line represents the water temperature measured with a thermocouple. Area between red lines represents the simmering range.

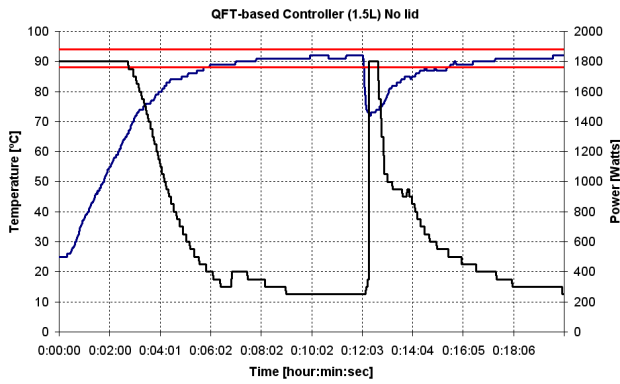


Fig. 20. Experimental results obtained with the fixed QFT-based controller. It has to heat up 1.5 liters of water to the simmering range. Besides, 0.5 liters of water are added at $t=12:15$. The pot is not covered with a lid. Blue line represents the water temperature measured with a thermocouple. Area between red lines represents the simmering range.

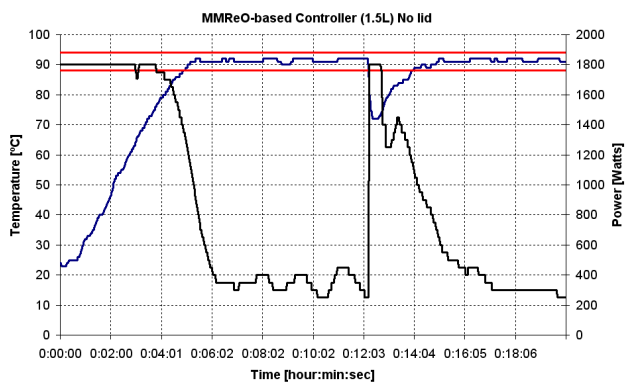


Fig. 23. Experimental results obtained with the adaptive MMReO-based controller. It has to heat up 1.5 liters of water to the simmering range. Besides, 0.5 liters of water are added at $t=12:10$. The pot is not covered with a lid. Blue line represents the water temperature measured with a thermocouple. Area between red lines represents the simmering range.

VI. CONCLUSION

This paper has shown the potential of the reset observers applied to process control. Specifically, Multiple-Model Reset Observer (MMReO) has been applied to water temperature control for induction cooker, which guarantees a proper food cooking, and allows to perform more complicated cooking processes such as simmering.

Since the amount of water and food are initially unknown, a previously developed analytical model has been used to characterize the uncertainty of the process, simplifying the design and tuning of the proposed MMReO. For comparison purposes, a fixed robust QFT-based controller has also been designed.

Both proposed controller meet all user requirements such as a low settling time, an accurate temperature control within the simmering range, and fast disturbance rejection. The adaptive controller based on MMReO has shown a higher performance compared with the fixed QFT-based controller. Depending on the initial amount of water, up to a 30% time saving is achieved by using the adaptive controller based on MMReO. The rationale behind this is that it can identify the system parameters on line so that the uncertainty of the process is significantly decreased. On the other hand, since the effectiveness of the adaptive controller relies on the number of fixed identification models of the MMReO, its computational cost is higher compared with the fixed QFT-based controller. Although this drawback, the adaptive controller based on MMReO is preferred because of its superior performance.

Independently of the implemented controller, the resultant control scheme is robust, safe, and very user friendly. Eventually, it could be applied in domestic induction hobs for automatic cooking.

REFERENCES

- [1] J. Acero, J. M. Burdio, L. A. Barragan, D. Navarro, R. Alonso, J. R. Garcia, F. Monterde, P. Hernandez, S. Llorente, and I. Garde. Domestic induction appliances. *IEEE Industry Applications Magazine*, 16(2):39–47, 2010.
- [2] J. M. Burdio, F. Monterde, J. R. Garcia, L. A. Barragan, and A. Martinez. A two-output series-resonant inverter for induction-heating cooking appliances. *IEEE Trans. on Power Electronics*, 20(4):815–822, 2005.
- [3] I. Millan, D. Puyal, J. M. Burdio, C. Bernal, and J. Acero. Improved performance of half-bridge series resonant inverter for induction heating with discontinuous mode control. In *Proc. IEEE Applied Power Electronics Conference and Exposition (APEC)*, pages 1293–1298, 2007.
- [4] C. Carretero, J. Acero, R. Alonso, J. M. Burdio, and F. Monterde. Temperature influence on equivalent impedance and efficiency of inductor systems for domestic induction heating appliances. In *Proc. IEEE Applied Power Electronics Conference and Exposition (APEC)*, pages 153–158, 2007.
- [5] D. Paesa, S. Llorente, C. Sagues, and O. Aldana. Adaptive observers applied to pan temperature control of induction hobs. *IEEE Trans. on Industry Applications*, 45(3):1116–1125, 2009.
- [6] U. Has, J. Schieferdecker, and D. Wassilew. Infrared sensor to control temperature of pans on consumer hobs. In *Proc. Int. Congr. OPTO*, pages 247–250, 1998.
- [7] U. Has, J. Schieferdecker, and D. Wassilew. Temperature control for food in pots on cooking hobs. *IEEE Trans. on Industrial Electronics*, 46(5):1030–1034, 1999.
- [8] C. Franco, D. Paesa, C. Sagues, and S. Llorente. Analytical modeling of a saucepan in an induction hob. In *Proc. of the 18th IEEE Mediterranean Control Conference*, pages 298–303, 2010.
- [9] K. S. Narendra and A. M. Annaswamy. *Stable Adaptive Systems*. Dover Publications, 2005.
- [10] D. Koenig. Unknown input proportional multiple-integral observer design for linear descriptor systems: application to state and fault estimation. *IEEE Trans. on Automatic Control*, 50(2):212–217, 2005.
- [11] M. Athans, D. Castanon, K. Dunn, C. Greene, L. Wing, N. Sandell, and A. Willsky. The stochastic control of the F-8C aircraft using a multiple model adaptive control (MMAC) method-Part I: Equilibrium flight. *IEEE Trans. on Automatic Control*, 22(5):768–780, 1977.
- [12] K. S. Narendra and J. Balakrishnan. Adaptive control using multiple models. *IEEE Trans. on Automatic Control*, 42(2):171–187, 1997.
- [13] S. Fekri, M. Athans, and A. Pascoal. RMMAC: A novel robust adaptive control scheme - Part I: Architecture. In *Proc. of the IEEE Conference on Decision and Control*, pages 1134–1139, 2004.
- [14] D. Paesa, C. Franco, S. Llorente, G. Lopez-Nicolas, and C. Sagues. Reset adaptive observers and stability properties. In *Proc. of the 18th IEEE Mediterranean Control Conference*, pages 1435–1440, 2010.
- [15] Horowitz I.M. A synthesis theory for linear time-varying feedback systems with plant uncertainty. *IEEE Trans. on Automatic Control*, 20(4):454–464, 1975.
- [16] Z. Liu, F. L. L. Luo, and M. H. Rashid. QFT-based robust and precision motion control system for a high speed direct-drive XY table positioning mechanism. In *Proc. of the IEEE Industry Applications Society Annual Meeting*, volume 1, pages 293–300, 2003.
- [17] C. Lucas, M. M. Shahnehchi, P. Asadi, and P. M. Rad. A robust speed controller for switched reluctance motor with nonlinear QFT design approach. In *Proc. of the IEEE Industry Applications Society Annual Meeting*, volume 3, pages 1573–1577, 2000.
- [18] D. Paesa, C. Franco, S. Llorente, G. Lopez-Nicolas, and C. Sagues. QFT-based robust simmering control for domestic induction cookers using an infrared sensor. In *Proc. of the 45th IEEE Industry Applications Society Annual Meeting*, October 2010.
- [19] O. Yaniv. *Quantitative Feedback Design of Linear and Nonlinear Control Systems*. Kluwer Academic Publishers, 1999.
- [20] Chait Y. and Yaniv O. Multiple-input/single-output computer-aided control design using the quantitative feedback theory. *Int. Journal of Robust and Nonlinear Control*, 3(1):47–54, 1993.
- [21] A. Banos. Nonlinear quantitative feedback theory. *Int. Journal of Robust and Nonlinear Control*, 17(2):181–202, 2007.
- [22] J. Acero, D. Navarro, L. A. Barragan, I. Garde, and J. M. Burdio. FPGA-based power measuring for induction heating appliances using sigma-delta A/D conversion. *IEEE Trans. on Power Electronics*, 54(4):1843–1852, 2007.
- [23] O. Lucia, J. M. Burdio, I. Millan, J. Acero, and D. Puyal. Load-adaptive control algorithm of half-bridge series resonant inverter for domestic induction heating. *IEEE Trans. on Power Electronics*, 56(8):3106–3116, 2009.